

## Matter-wave dromions in a disk-shaped dipolar Bose-Einstein condensate with the Lee-Huang-Yang correction

Zeyun Shi<sup>1,2</sup> and Guoxiang Huang<sup>2,3,4</sup>

<sup>1</sup>*School of Electrical and Information Engineering, Hubei University of Automotive Technology, Shiyan 442000, China*

<sup>2</sup>*State Key Laboratory of Precision Spectroscopy, East China Normal University, Shanghai 200241, China*

<sup>3</sup>*NYU-ECRU Joint Institute of Physics, New York University at Shanghai, Shanghai 200062, China*

<sup>4</sup>*Collaborative Innovation Center of Extreme Optics, Shanxi University, Taiyuan 030006, China*

 (Received 30 September 2022; revised 13 January 2023; accepted 10 February 2023; published 23 February 2023)

We investigate, both analytically and numerically, the nonlinear dynamics of (2+1)-dimensional [(2+1)D] matter waves excited in a disk-shaped dipolar Bose-Einstein condensate (BEC) when quantum fluctuations described by the Lee-Huang-Yang (LHY) correction are taken into consideration. By using a method of multiple scales, we derive Davey-Stewartson I equations that govern the nonlinear evolution of matter-wave envelopes. We demonstrate that the system supports (2+1)D matter-wave dromions, which are superpositions of a short-wavelength excitation and a long-wavelength mean flow. We found that the stability of the matter-wave dromions can be enhanced by the LHY correction. We also found that such dromions display interesting behaviors of collision, reflection, and transmission when they interact with each other and are scattered by obstacles. The results reported here are useful not only for improving the understanding on the physical property of the quantum fluctuations in BECs, but also for possible experimental findings of new nonlinear localized excitations in systems with long-ranged interactions.

DOI: [10.1103/PhysRevE.107.024214](https://doi.org/10.1103/PhysRevE.107.024214)

### I. INTRODUCTION

In the past decades, the remarkable experimental realization of Bose-Einstein condensates (BECs) in weakly interacting cold atomic gases opened a new avenue for the exploration of nonlinear properties of matter waves. The most significant experimental progress includes demonstrations of the matter-wave four-wave mixing, superradiance, amplification, and collapse [1–4]. These studies established a new field of nonlinear atom optics that deals with various nonlinear dynamics of matter-wave excitations [5–7].

Fascinating phenomena of solitons and related excitations occur in many nonlinear media (e.g., fluids, plasmas, solids, optical fibers, etc.), and have potential applications in information processing and transmission [8]. Solitonlike nonlinear localized excitations in BECs (called matter-wave solitons generally) have also received much attention. Related studies focused mainly on solitons in BECs with contact atom-atom interactions, controlled by Gross-Pitaevskii (GP) equations with local cubic nonlinearity, by which stable bright (dark) solitons for attractive (repulsive) interatomic interaction can be obtained in one dimension [9–12].

In order to obtain new and more interesting properties, in recent years there has been considerable interest in exploring cold atomic gases with more rich atom-atom interactions. In particular, nonlocal (long-ranged) dipole-dipole interaction has been suggested to realize a novel kind of degenerate quantum gas both in the weakly interacting limit and also in strongly correlated regimes. It has been shown that BECs

with dipole-dipole interaction, governed by GP equations with nonlocal cubic nonlinearity, can support high-dimensional solitons. However, generally such solitons can only be stabilized by some special conditions due to the fact that the dipole-dipole interaction is anisotropic and nonpositive definite [13–20].

In the studies mentioned above, the ground-state energy of BECs was obtained by using a mean-field approximation. Going beyond this approximation gives a Lee-Huang-Yang (LHY) correction [21], which is originated from the quantum fluctuations in the BEC. The LHY correction can stabilize the BEC against the mean-field collapse, which has been observed in Bose-Bose mixtures and also in dipolar BECs, and has been shown to be useful for the formation of solitonlike quantum droplets and supersolid crystals [22–28].

Stable high-dimensional solitons are rarely found in nature. The reason is that it is usually not easy to realize the balance among nonlinearity, dispersion, and/or diffraction. Nevertheless, if a system is prepared under particular conditions the nonlinear dynamics of wave envelopes can be effectively described by some integrable (or nearly integrable) nonlinear partial differential equations, and one is able to observe high-dimensional solitons during propagation in the system [29]. In Ref. [30], (2+1)-dimensional [(2+1)D] [31] weak nonlinear matter waves excited from the background of a disk-shaped BEC with local atom-atom interaction were considered, Davey-Stewartson I (DSI) equations were derived, and hence dromionlike (2+1)D soliton excitations were proved to be possible. Predicted first by Boiti *et al.* [32], a dromion (the name was first given in Ref. [33]) is a

(2+1)D nonlinear localized excitation with two wave components; one describes a short-wavelength excitation decaying in two spatial directions and another one describes a long-wavelength mean flow generated by the short-wavelength excitation [29,30,32–35].

In the present paper, we extend the study of Ref. [30] by investigating, both analytically and numerically, the nonlinear dynamics of matter waves excited in a disk-shaped BEC with dipole-dipole interatomic interaction. In order to include the contribution of the quantum fluctuations beyond mean-field approximation, the LHY correction term is taken into account in the GP equation describing the dipolar BEC. By using a standard asymptotic expansion method of multiple scales [36], we derive DSI equations that control the nonlinear evolution of two coupled matter-wave envelope components. We show that the system supports (2+1)D matter-wave dromions excited from the ground-state background of the dipolar BEC, which are superpositions of a short-wavelength excitation and a long-wavelength mean flow. We demonstrate that the stability of the matter-wave dromions can be enhanced significantly by the LHY correction. We also demonstrate that such (2+1)D nonlinear matter-wave dromions exhibit many interesting behaviors for collision, reflection, and transmission when they interact with each other and are scattered by obstacles. The results reported here are beneficial not only for a deep understanding on novel physical properties of the quantum fluctuations (the LHY correction) in BECs, but also for seeking possible experimental findings of new types of high-dimensional nonlinear localized excitations in systems with long-ranged interactions.

The remainder of the paper is arranged as follows. In Sec. II, we describe the physical model under study. In Sec. III, we derive the DSI equations, give the dromion solutions, and discuss their stability. In Sec. IV, we investigate the collision between two dromions, and discuss their reflection and transmission when scattered by obstacles. Finally, Sec. V contains the summary of our main results obtained in this paper.

## II. MODEL

We consider a dipolar BEC, which consists of  $N$  bosonic atoms interacting through short-ranged interaction (characterized by  $s$ -wave scattering length  $a_s$ ) and also long-ranged dipole-dipole interaction. The external potential that traps the atoms is disk shaped, as schematically shown in Fig. 1(a).  $\mathbf{R} = \mathbf{r} - \mathbf{r}'$  is the separation between two dipoles  $\mathbf{d}_1$  and  $\mathbf{d}_2$  [located respectively at  $\mathbf{r} = (x, y, z)$  and  $\mathbf{r}' = (x', y', z')$ ], with their interaction described by the dipole-dipole interaction potential  $U_{dd}(\mathbf{R}) = [1 - 3 \cos^2 \theta]/R^3$ . Here,  $\cos \theta = z/R$ ,  $R = |\mathbf{R}|$ , and  $\theta$  is the angle formed by the vector joining the two interacting particles and the dipole direction. The disk-shaped dipolar BEC is formed by tightly confining the atoms in the  $x$ - $y$  plane using a strong external harmonic confinement potential along the  $z$  direction, in which the dipoles (represented by arrows) are polarized at angle  $\alpha$  (with respect to the  $z$ -axis) in the  $x$ - $z$  plane; see the insets of Fig. 1(a).

At zero temperature and beyond mean-field approximation, the dipolar BEC can be described by the (3+1)-dimensional

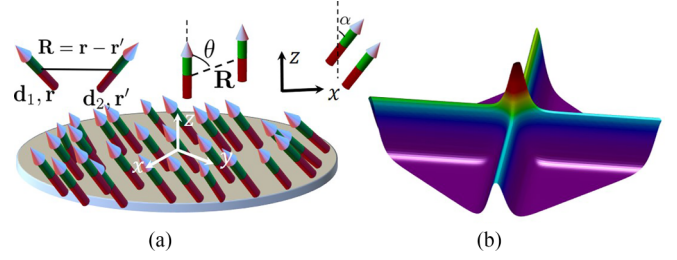


FIG. 1. (a) Dipolar BEC tightly confined in the  $xy$  plane by a strong harmonic confinement along the  $z$  direction. Two dipoles located respectively at position  $\mathbf{r}$  and  $\mathbf{r}'$  interact via the dipole-dipole interaction potential  $U_{dd}(\mathbf{R}) = [1 - 3 \cos^2 \theta]/R^3$ , with  $\cos \theta = z/R$ ,  $R = |\mathbf{R}|$ ,  $\mathbf{R} = \mathbf{r} - \mathbf{r}'$ ;  $\theta$  is the angle between the polarization direction and the relative position of the two dipoles (i.e.,  $\mathbf{R}$ ). Dipoles are assumed to be polarized in the  $x$ - $z$  plane, with a tilting angle  $\alpha$  with respect to the  $z$  axis. (b) Intensity of the matter-wave dromion in the disk-shaped dipolar BEC, which is a localized (2+1)D wave packet (short-wave component) riding on the crossing point of two antikinks (long-wave component).

GP equation [20,24,27]

$$i\hbar \frac{\partial \psi}{\partial t} = \left[ -\frac{\hbar^2}{2m} \nabla^2 + V(\mathbf{r}) + g_{3D} |\psi|^2 + g_{QF} |\psi|^3 + g_{dd} \int d^3 r' U_{dd}(\mathbf{r} - \mathbf{r}') |\psi(\mathbf{r}', t)|^2 \right] \psi. \quad (1)$$

Here  $\psi(\mathbf{r}, t)$  is an order parameter (satisfying the normalized condition  $\int d^3 r |\psi|^2 = N$ );  $\nabla^2 = \partial^2/\partial x^2 + \partial^2/\partial y^2 + \partial^2/\partial z^2$ ;  $d^3 r' = dx' dy' dz'$ ;  $g_{3D} = 4\pi \hbar^2 a_s/m$  is the short-ranged (contact) interaction parameter, with  $m$  the atomic mass and  $a_s$  the  $s$ -wave scattering length;  $g_{QF} \simeq 32/(3\sqrt{\pi}) g_{3D} a_s^{3/2} [1 + 3/2(a_{dd}/a_s)^2]$  is the parameter describing the quantum fluctuations, with  $a_{dd} = \mu_0 d^2 m / (12\pi \hbar^2)$  the dipolar length [20,24,27];  $g_{dd} = \mu_0 d^2 / (4\pi)$  is the parameter describing the nonlocal interaction, with  $\mu_0$  the permeability of free space and  $d$  the dipole moment. In Eq. (1),  $V(\mathbf{r}) = \frac{1}{2} m [\omega_{\perp}^2 (x^2 + y^2) + \omega_z^2 z^2]$  is the external trapping potential. Since the BEC is assumed to be strongly confined along the  $z$  direction, we have  $\omega_z \gg \omega_{\perp}$ , where  $\omega_{\perp}$  and  $\omega_z$  are trap frequencies in the  $xy$  plane and in the  $z$  axis, respectively.

Notice that in the present system there exist three types of contributions of interatomic interactions (i.e., the  $s$ -wave interaction, the interaction induced by the LHY correction, and the dipole-dipole interaction). Since the  $s$ -wave scattering length  $a_s$  can be tuned by optical Feshbach resonance [37,38], the term  $g_{3D} |\psi|^2$  can be positive or negative (which gives repulsive or attractive interactions correspondingly). The contribution by the quantum fluctuations in the BEC is represented by the LHY correction term  $g_{QF} |\psi|^3$ , which is local and can be positive and negative depending on the sign of  $a_s$ . The contribution by the nonlocal dipole-dipole interaction, represented by the term with the spatial integration  $g_{dd} \int d^3 r' U_{dd}(\mathbf{r} - \mathbf{r}') |\psi(\mathbf{r}', t)|^2$ , can also be positive or negative depending on the angle  $\theta$  and the relative position of dipoles. Notice also that the dipole-dipole interaction is not only anisotropic but also nonpositive definite. For example,

$U_{dd}(\mathbf{R}) = 1/R^3$  when  $\theta = \pi/2$  (i.e.,  $\cos\theta = 0$ );  $U_{dd}(\mathbf{R}) = -2/R^3$  when  $\theta = 0$  (i.e.,  $\cos\theta = 1$ ).

For the convenience of the following calculations, we introduce the dimensionless variables  $t = \tau_0 t_1$ ,  $\psi = \phi(N/l_z^3)^{1/2}$ ,  $\vec{\zeta} = (x_1, y_1, z_1) = (x, y, z)/l_z$ ,  $a_s = \tilde{a}_s l_z$ , and  $a_{dd} = \tilde{a}_{dd} l_z$ . Here  $\tau_0 = ml_z^2/\hbar$ , with  $l_z \equiv \sqrt{\hbar/(m\omega_z)}$  the harmonic oscillator length in the  $z$  direction. Then Eq. (1) is cast into the dimensionless form

$$i\frac{\partial\phi}{\partial t_1} = \left[ -\frac{1}{2}\tilde{\nabla}^2 + V(\vec{\zeta}) + 4\pi\tilde{a}_s N|\phi|^2 + WN^{3/2}|\phi|^3 + 3N\tilde{a}_{dd} \int d^3\zeta' U_{dd}(\vec{\zeta} - \vec{\zeta}')|\phi(\vec{\zeta}', t_1)|^2 \right] \phi, \quad (2)$$

where  $\tilde{\nabla}^2 = \partial^2/\partial x_1^2 + \partial^2/\partial y_1^2 + \partial^2/\partial z_1^2$ ,  $d^3\zeta = dx_1 dy_1 dz_1$ ,  $V(\vec{\zeta}) = \frac{1}{2}\tau_0^2[\omega_\perp^2(x_1^2 + y_1^2) + \omega_z^2 z_1^2] \equiv V_\perp(x_1, y_1) + V_{z_1}(z_1)$ , and  $W = \frac{128}{3}\sqrt{\pi}\tilde{a}_s^{5/2}[1 + 3(\tilde{a}_{dd}/\tilde{a}_s)^2/2]$ .

Since the axial trapping potential has been assumed to be strong, the motion of wave function  $\phi$  in the  $z_1$  direction is frozen into the ground state of the harmonic potential  $V_{z_1}(z_1) = \tau_0^2 \omega_z^2 z_1^2/2$ . Thereby we can make the approximation  $\phi(\vec{\zeta}, t_1) \approx \varphi(\vec{\rho}, t_1)\phi_0(z_1)$ , where  $\phi_0(z_1) \equiv (1/\sqrt[3]{\pi})\exp(-z_1^2/2)$  is the ground-state wave function of the potential  $V_{z_1}(z_1)$  and  $\varphi(\vec{\rho}, t_1)$  [ $\vec{\rho} \equiv (x_1, y_1)$ ] is the two-dimensional (2D) wave function in the  $x_1$ - $y_1$  plane. After multiplying  $\phi_0(z_1)$  and integrating over  $z_1$ , Eq. (2) is converted into the effective (2+1)D GP equation

$$i\frac{\partial\varphi}{\partial t_1} = \left[ -\frac{1}{2}\tilde{\nabla}_\perp^2 + b + V_0|\bar{\rho}|^2 + w_1|\varphi|^2 + w_2|\varphi|^3 + g \int d^2\rho' U_{2D}(\vec{\rho} - \vec{\rho}')|\varphi(\vec{\rho}')|^2 \right] \varphi, \quad (3)$$

where  $d^2\rho' = dx_1' dy_1'$ ,  $b = ml_z^2 \omega_z^2/4 + \hbar^2/(4ml_z^2)$ ,  $V_0 = \frac{1}{2}\omega_\perp^2 \tau_0^2$ ,  $w_1 = 2\sqrt{2\pi}N\tilde{a}_s$ ,  $w_2 = N^{3/2}\sqrt{2/5}\frac{128}{3}\pi^{-1/4}\tilde{a}_s^{5/2}[1 + \frac{3}{2}(\tilde{a}_{dd}/\tilde{a}_s)^2]$  (a nonlinear parameter characterizing the quantum fluctuations, called the LHY parameter below), and  $g = 3\tilde{a}_{dd}N$ .  $U_{2D}(\vec{\rho} - \vec{\rho}')$  is calculated in momentum space by using the convolution integral, as done in Refs. [39–41]. The dipole at position  $(x_1, y_1)$  polarizes at angle  $\alpha$  to the  $z_1$  axis in the  $x_1$ - $z_1$  plane [see the inset of Fig. 1(a)]. The constant  $b$  in Eq. (3) can be removed by using the transformation  $\varphi(\vec{\rho}, t_1) \rightarrow \varphi(\vec{\rho}, t_1)e^{-ibt_1}$ . Then we have

$$i\frac{\partial\varphi}{\partial t_1} = \left[ -\frac{1}{2}\tilde{\nabla}_\perp^2 + V_0|\bar{\rho}|^2 + w_1|\varphi|^2 + w_2|\varphi|^3 + g \int d^2\rho' U_{2D}(\vec{\rho} - \vec{\rho}')|\varphi(\vec{\rho}')|^2 \right] \varphi. \quad (4)$$

The model described above is quite general, valid for any dipolar BECs trapped by a disk-shaped potential. Here we take the  $^{164}\text{Dy}$  BEC [24,42] as an example to facilitate the calculation and discussion given below. The system parameters are given by  $d = 10 \mu_B = 9.274 01 \times 10^{-23} \text{ A m}^2$  (magnetic-dipole moment),  $\mu_0 = 4\pi \times 10^{-7} \text{ N/m}^2$ ,  $a_{dd} = 132.7a_0 = 7.02 \times 10^{-9} \text{ m}$  (dipolar length),  $a_s = 100a_0 = 5.292 \times 10^{-9} \text{ m}$  (scatter length),  $\omega_z = 2\pi \times 62.6 \text{ Hz}$  (trap frequency),

$l_z = 45\pi a_{dd} \simeq 1 \mu\text{m}$  (harmonic oscillator length in the  $z$  direction), and  $\tau_0 = 2.5 \text{ ms}$ .

### III. AMPLITUDE EQUATIONS, MATTER-WAVE DROMIONS, AND THEIR STABILITY

#### A. Amplitude equations

We now investigate the weak nonlinear excitations in the system based on the effective GP equation (4). Note that each term of the three nonlinear terms in Eq. (4) can be either positive (repulsive) or negative (attractive). Thus, generally speaking, the whole nonlinearity in Eq. (4) may be positive or negative, depending on the signs and relative magnitudes of  $w_1$ ,  $w_2$ , and  $U_{2D}(\vec{\rho})$ . By taking  $N = 2 \times 10^5$  and  $\alpha = 0$  ( $\alpha$  is the tilting angle of the dipoles with respect to the  $z$  axis), and using the system parameters given in the previous section, we can obtain  $w_1 > 0$ ,  $w_2 > 0$ , and  $U_{2D}(\vec{\rho}) > 0$ . In this situation, the whole nonlinearity is repulsive and hence the system supports dromion solutions. Moreover, we assume also that the transverse trapping frequency  $\omega_\perp$  is small (i.e., the disk radius is large). This means that the transverse trapping potential  $V_0|\bar{\rho}|^2$  in Eq. (4) plays no significant role if one is not interested in the case for dromions excited near the boundary or interacting with the boundary of the BEC. Hence, we shall neglect the small transverse trapping potential in the following calculations. Under such assumptions, the ground-state solution  $\varphi_0$  of Eq. (4) is a uniform one, i.e.,  $\varphi_0 = u_0 \exp(-i\mu t_1)$ . Here  $\mu = u_0^2[w_1 + u_0 w_2 + g \iint U_{2D}(\vec{\rho}) d^2\rho]$ , with  $u_0$  a constant.

To study the soliton phenomenon in a complicated nonlinear system, a convenient method is to derive the amplitude equations [like the DS equations (9a) and (9b) obtained below] that govern the spatial-temporal evolution of the envelopes of nonlinear excitations by using asymptotic expansions. Such a method is powerful and has been widely employed in nonlinear wave theory [29,36]. Here, to investigate the dromion excitations generated from the ground-state background  $\varphi_0$  of the dipolar BEC, we apply the method of multiple scales [36] to derive relevant amplitude equations. The general solution can be written as the form  $\varphi = [u_0 + \varphi_p(x_1, y_1, t_1)] \exp(-i\mu t_1)$ , with  $\varphi_p$  denoting the excitation from the ground state. Taking  $\varphi(\vec{\rho}, t_1) = P(\vec{\rho}, t_1) \exp[-i\mu t_1 + i\tilde{\varphi}(\vec{\rho}, t_1)]$ , Eq. (4) becomes

$$\frac{\partial P}{\partial t_1} + \nabla P \cdot \nabla \tilde{\varphi} + \frac{1}{2}\nabla^2 \tilde{\varphi} = 0, \quad (5a)$$

$$P \frac{\partial \tilde{\varphi}}{\partial t_1} - \frac{1}{2}\nabla^2 P - \mu P + \frac{1}{2}P|\nabla \tilde{\varphi}|^2 + w_2 P^4 + P \int R(\vec{\rho} - \vec{\rho}') P^2(\vec{\rho}') d^2\rho' = 0, \quad (5b)$$

where  $\vec{\rho} = (x_1, y_1)$ ,  $\vec{\rho}' = (x_1', y_1')$ ,  $d^2\rho' = dx_1' dy_1'$ , and  $R(\vec{\rho}) \equiv gU_{2D}(\vec{\rho}) + w_1\delta(\vec{\rho})$ . To solve Eq. (5), we make the asymptotic expansions  $P = u_0 + \epsilon a_1 + \epsilon^2 a_2 + \epsilon^3 a_3 + \dots$  and  $\tilde{\varphi} = \epsilon \phi_1 + \epsilon^2 \phi_2 + \epsilon^3 \phi_3 + \dots$ . Here  $a_j$  and  $\phi_j$  ( $j = 1, 2, 3, \dots$ ) are functions of the multiscale variables  $\theta = \beta x_1 - \omega t_1$ ,  $\tau = \epsilon^2 t_1$ ,  $\xi = \epsilon(x_1/v_g - t_1)$ , and  $\eta = \epsilon y_1$ ;  $\epsilon$  is a small parameter characterizing the amplitude of the excitation from the BEC ground state. Substituting these

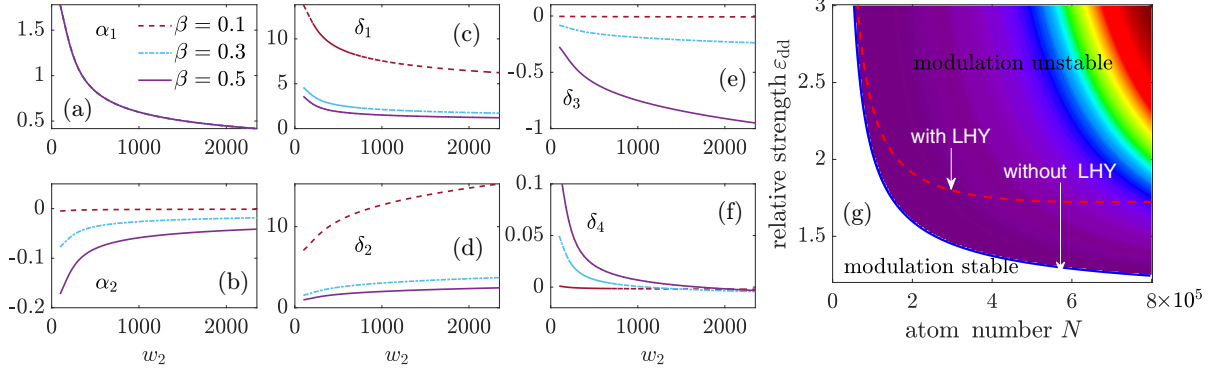


FIG. 2. (a)–(f) Coefficients  $\alpha_j$  ( $j = 1, 2$ ) and  $\delta_l$  ( $l = 1, 2, 3, 4$ ) in Eqs. (9a) and (9b) as functions of the LHY parameter  $w_2$  for different wave number of the excitation  $\beta = 0.1$  (dotted red line),  $\beta = 0.3$  (dashed blue line), and  $\beta = 0.5$  (solid purple line). (g) Phase diagram for the existence of matter-wave dromions in the  $N$ - $\epsilon_{dd}$  plane ( $\epsilon_{dd} \equiv a_{dd}/a_s$  is relative dipole strength). Here the dashed red (solid blue) line denotes the boundary between the modulational instability (MI) and the modulational stability (MS) of the BEC ground state in the presence (absence) of the LHY correction. The existence of the LHY term enlarges the region where the BEC ground state is modulationally stable.

expansions into Eqs. (5), we obtain perturbation equations for  $a_j$  and  $\phi_j$ , which can be solved order by order.

At the first-order approximation ( $j = 1$ ), we have the solution

$$a_1 = i \frac{u_0 \beta^2}{2\omega} A_1 e^{i\theta} + c.c., \quad (6)$$

$$\phi_1 = A_0 + (A_1 e^{i\theta} + c.c.). \quad (7)$$

The linear dispersion relation is given by  $\omega = \omega(\beta)$  ( $\beta$  and  $\omega$  are the wave number and frequency of the excitation, respectively), with

$$\omega = \left[ \frac{1}{4} \beta^4 + u_0^2 \beta^2 \hat{R}(\beta) + \frac{3}{2} w_2 u_0^3 \beta^2 \right]^{1/2}. \quad (8)$$

Here  $\hat{R}(\beta)$  is the Fourier transform of  $R(\vec{\rho})$ .  $A_1$  and  $A_0$  are respectively the amplitude (envelope) of the short wave and that of the long wave (mean flow), both of which are functions of the slow variables  $\xi$ ,  $\eta$ , and  $\tau$ , yet to be determined.

Going to the third-order approximation ( $j = 3$ ), we obtain the DS equations describing the interaction between the long wave  $A_0$  and the short wave  $A_1$ :

$$\alpha_1 \frac{\partial^2 A_0}{\partial \xi^2} - \frac{\partial^2 A_0}{\partial \eta^2} = -\alpha_2 \frac{\partial |A_1|^2}{\partial \xi}, \quad (9a)$$

$$i \frac{\partial A_1}{\partial \tau} + \left( \delta_1 \frac{\partial^2}{\partial \xi^2} + \delta_2 \frac{\partial^2}{\partial \eta^2} \right) A_1 + \delta_3 |A_1|^2 A_1 = -\delta_4 A_1 \frac{\partial A_0}{\partial \xi}. \quad (9b)$$

In these equations, the terms with the second-order derivatives  $\partial^2/\partial \xi^2$  and  $\partial^2/\partial \eta^2$  describe the dispersion and diffraction effects, and the term  $|A_1|^2 A_1$  describes the nonlinear effect of the system. From Eq. (9a), we see that the self-interaction of the short-wave component (the term on the right-hand side of the equation)  $A_1$  supports the occurrence of the long-wave component  $A_0$ ; however, the long-wave component  $A_0$  has a backaction to the short-wave component  $A_1$ , which is reflected by the term on the right-hand side of Eq. (9b). The detailed derivation of the DS equations (9a) and (9b) and

explicit expressions of their coefficients  $\alpha_j$  ( $j = 1, 2$ ) and  $\delta_l$  ( $l = 1, 2, 3, 4$ ) are presented in Appendix A.

Before proceeding, we give a simple discussion on the role played by the LHY correction [characterized by the LHY parameter  $w_2$  in Eqs. (4) and (5)] to the coefficients of the DS equations (9a) and (9b). Shown in Figs. 2(a)–2(f) are coefficients  $\alpha_j$  ( $j = 1, 2$ ) and  $\delta_l$  ( $l = 1, 2, 3, 4$ ) in Eqs. (9a) and (9b) as functions of the parameter  $w_2$  (the strength of LHY correction), for different wave number of the excitation from the ground-state background of the BEC. The dotted red line, dashed blue line, and solid purple line in the figures are for  $\beta = 0.1$ ,  $0.3$ , and  $0.5$ , respectively. We see that these coefficients display the following characters.

(i)  $\alpha_1$  ( $\alpha_2$ ) is decreased (increased) as  $w_2$  grows;  $\alpha_2$  has a weak dependence on  $\beta$ , but  $\alpha_1$  is nearly invariant when  $\beta$  is changed.

(ii)  $\delta_1$  is reduced as  $w_2$  increases, while  $\delta_2$  is increased if  $w_2$  is increased.

(iii) Both  $\delta_3$  and  $\delta_4$  decrease when  $w_2$  increases.

These results tell us that the coefficients in the DS equations (9a) and (9b) have strong dependence on the LHY correction of the system; moreover, these coefficients are adjustable, providing a flexible way to manipulate the system so that stable matter-wave dromions are possible, as explained in the following section.

## B. Matter-wave dromions and their stabilities

Now we investigate possible high-dimensional solitons solutions based on the DS equations (9a) and (9b). As mentioned above, due to the anisotropic and nonpositive definite dipole-dipole interaction, the high-dimensional solitons in dipolar BECs are generally unstable. However, under some conditions, the dipole-dipole interaction can be made isotropic and has a definite sign, and hence the system can support stable solitons. Based on the assumptions given at the beginning of the last subsection, the nonlinearity of the system is repulsive isotropically. In this case, the ground-state background

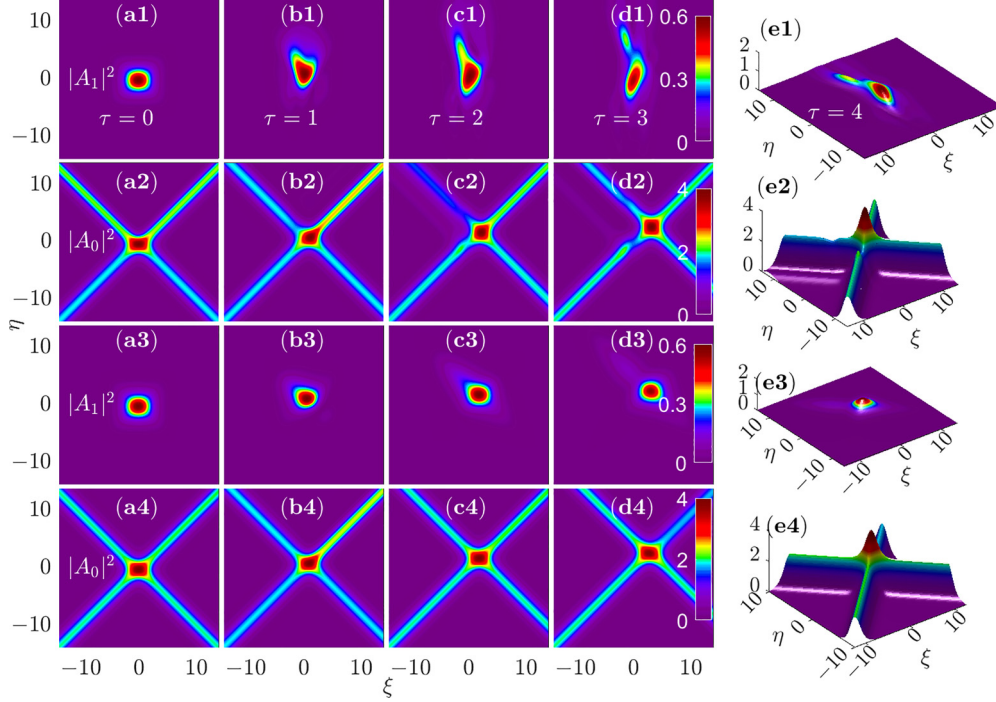


FIG. 3. Matter-wave dromions in the dipolar BEC obtained by numerically solving the DS equations (9a) and (9b) for different times  $\tau = 0, 1, 2, 3, 4$ , respectively. The data in the figure are normalized to 1, all of which share the same color bar. (a1)–(e1) The distribution of the short-wave component  $|A_1|^2$  as functions of  $\xi$  and  $\eta$  in the absence of the LHY correction (i.e., the LHY parameter  $w_2 = 0$ ). (a2)–(e2) The same as (a1)–(e1) but for the long-wave component  $|A_0|^2$ . (a3)–(e3) The distribution of the short-wave component  $|A_1|^2$  as functions of  $\xi$  and  $\eta$  in the presence of the LHY term (i.e.,  $w_2 = 472.8$ ). (a4)–(e4) The same as (a3)–(e3) but for the long-wave component  $|A_0|^2$ . These results show that the LHY term can stabilize the dromions in the dipolar BEC greatly.

of the dipolar BEC is modulationally stable under the action of perturbations; the system allows the existence of dromion excitations that are excited on the ground-state background [30].

In order to determine the parameter domain for the existence of dromions, a modulational instability (MI) [43–46] analysis is carried out. Figure 2(g) shows the numerical result of the MI analysis, in which the phase diagram for the existence of dromions is illustrated in the  $N$ - $\varepsilon_{dd}$  plane ( $\varepsilon_{dd} \equiv a_{dd}/a_s$  is a parameter characterizing the relative dipole strength). In the figure, the dashed red (solid blue) line is the boundary between the MI and modulational stability (MS) in the presence (absence) of the LHY correction. We see that the domain in which the MS occurs (i.e., the modulation of the BEC ground state is stable) is increased by the existence of the LHY correction [represented by the parameter  $w_2$  in Eq. (4)], which means that the the LHY correction by the quantum fluctuations can make the existence domain of dromions enlarged significantly [47]. Note that the effect of the LHY term on the enlargement of the MS domain for large  $N$  is more significant than that for small  $N$ . This is due to the fact that the nonlinear coefficients describing the contact and dipolar interactions (i.e.,  $w_1$  and  $g$ ) are proportional to  $N$ , while the nonlinear coefficient describing the LHY correction ( $w_2$ ) is proportional to  $N^{3/2}$ .

We now present approximated soliton solutions for the DS equations (9a) and (9b). Using the transformation  $\partial A_0/\partial \xi = \delta_1/(\alpha_1 \delta_4) s$ ,  $A_1 = 2\sqrt{\delta_1/(\alpha_2 \delta_4)} u$ ,  $x' = \sqrt{\alpha_1} \xi$ ,  $y' = \eta$ , and  $t_2 = (\alpha_1/\delta_1) \tau$ , (9a) and (9b)

become

$$\frac{\partial^2 s}{\partial x'^2} - \frac{\partial^2 s}{\partial y'^2} + 4 \frac{\partial^2 |u|^2}{\partial x'^2} = 0, \quad (10a)$$

$$i \frac{\partial u}{\partial t_2} + \left( \frac{\partial^2}{\partial x'^2} + \frac{\partial^2}{\partial y'^2} \right) u + 2|u|^2 u + s u = \kappa_1 \frac{\partial^2 u}{\partial y'^2} + \kappa_2 |u|^2 u, \quad (10b)$$

with  $\kappa_1 = 1 - \alpha_1 \delta_2 / \delta_1$  and  $\kappa_2 = 2 - 4\alpha_1 \delta_3 / (\alpha_2 \delta_4)$ . To find analytic solutions, we assume the wave number  $\beta$  is small, which makes  $\kappa_1$  and  $\kappa_2$  play negligible roles. For instance, by taking  $\beta = 0.1$ , one has  $\kappa_1 = 0.006$  and  $\kappa_2 = -0.03$ . When taking  $\kappa_1 = \kappa_2 = 0$ , (10a) and (10b) reduce into standard DSI equations, which admit the dromion solution [29]:

$$u = \frac{\varrho}{F} \exp(\eta_1 + \eta_2), \quad s = 4 \frac{\partial^2 \ln F}{\partial x'^2}, \quad (11)$$

with  $F = F[\eta_1, \eta_2] \equiv 1 + \exp(\eta_1 + \eta_1^*) + \exp(\eta_2 + \eta_2^*) + \gamma \exp(\eta_1 + \eta_1^* + \eta_2 + \eta_2^*)$ ,  $\eta_1 = (k_r + ik_i)(x' + y')/2 + (\Omega_r + i\Omega_i)t'$ ,  $\eta_2 = (l_r + il_i)(y' - x')/2 + (\omega_r + i\omega_i)t'$ ,  $\Omega_r = -2k_r k_i$ ,  $\omega_r = -2l_r l_i$ ,  $\Omega_i + \omega_i = k_r^2 + l_r^2 - k_i^2 - l_i^2$ , and  $\varrho = 2\sqrt{2k_r l_r (\gamma - 1)} \exp(i\phi_\rho)$ . Here  $k_r$ ,  $k_i$ ,  $l_r$ ,  $l_i$ ,  $\gamma$ , and  $\phi_\rho$  are free real parameters. Shown in Fig. 1(b) is the intensity of the matter-wave dromion by taking  $k_r = 1$ ,  $k_i = 0.5$ ,  $l_r = 1$ ,  $l_i = 0.5$ ,  $\gamma = 3$ , and  $\phi_\rho = 0$ . In the figure, the hump in the center represents the localized (2+1)D wave packet (i.e., the short-wave component  $|u|^2$ ), which rides on the crossing point of the two antikinks (i.e., the long-wave component  $|s|^2$ ).

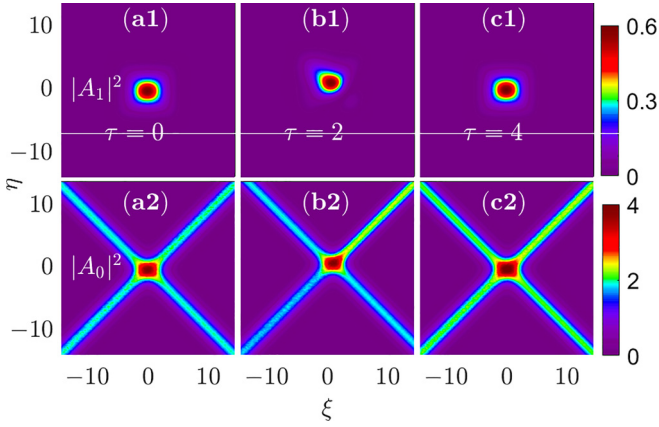


FIG. 4. Dynamical stability of the matter-wave dromion. Shown are intensity distributions of the short-wave component  $|A_1|^2$  (a1)–(c1) and the long-wave component  $|A_0|^2$  (a2)–(c2) of the dromion, as functions of  $\xi$  and  $\eta$  for  $\tau = 0, 1, 2$ , respectively, perturbed by 10% noise.

A numerical simulation is carried out for checking the validity of the above approximated solution given above. Figure 3 shows the propagation of the matter-wave dromion obtained by numerically solving the DS equations (9a) and

(9b) for different dimensionless times  $\tau = 0, 1, 2, 3, 4$ , respectively, by taking (11) as an initial condition. Illustrated in panels (a1)–(e1) is the distribution of the short-wave component  $|A_1|^2$  as functions of  $\xi$  and  $\eta$ ; the distribution in Figs. 3(a2)–3(e2) is the same as that in Figs. 3(a1)–3(e1) but for the long-wave component  $|A_0|^2$ . In the simulation, the system parameters used are  $k_r = l_r = 1.0$ , and  $k_i = l_i = 0.5$ , with  $w_2 = 0$  (i.e., the LHY correction is absent). We see that in the short-wave component a small side wave packet is generated; the two antikinks in the long-wave component are broken off after propagating to some distance. Thus, in the absence of the LHY correction, both the short- and long-wave components of the dromion are unstable during propagation.

To see what is the situation for the dromion propagation when the LHY correction is present, an additional simulation is made by using a nonzero  $w_2$ . Shown in Figs. 3(a3)–3(e3) and 3(a4)–3(e4) are respectively the distributions of  $|A_1|^2$  and  $|A_0|^2$  as functions of  $\xi$  and  $\eta$ , by taking  $w_2 = 472.8$ . We see that both the short- and long-wave components are rather robust in the course of their propagations. Therefore, the LHY correction beyond mean-field approximation contributed by the quantum fluctuations can stabilize the matter-wave dromion in the system.

To further check the dynamical stability of the dromion in the presence of the LHY correction, we have made a

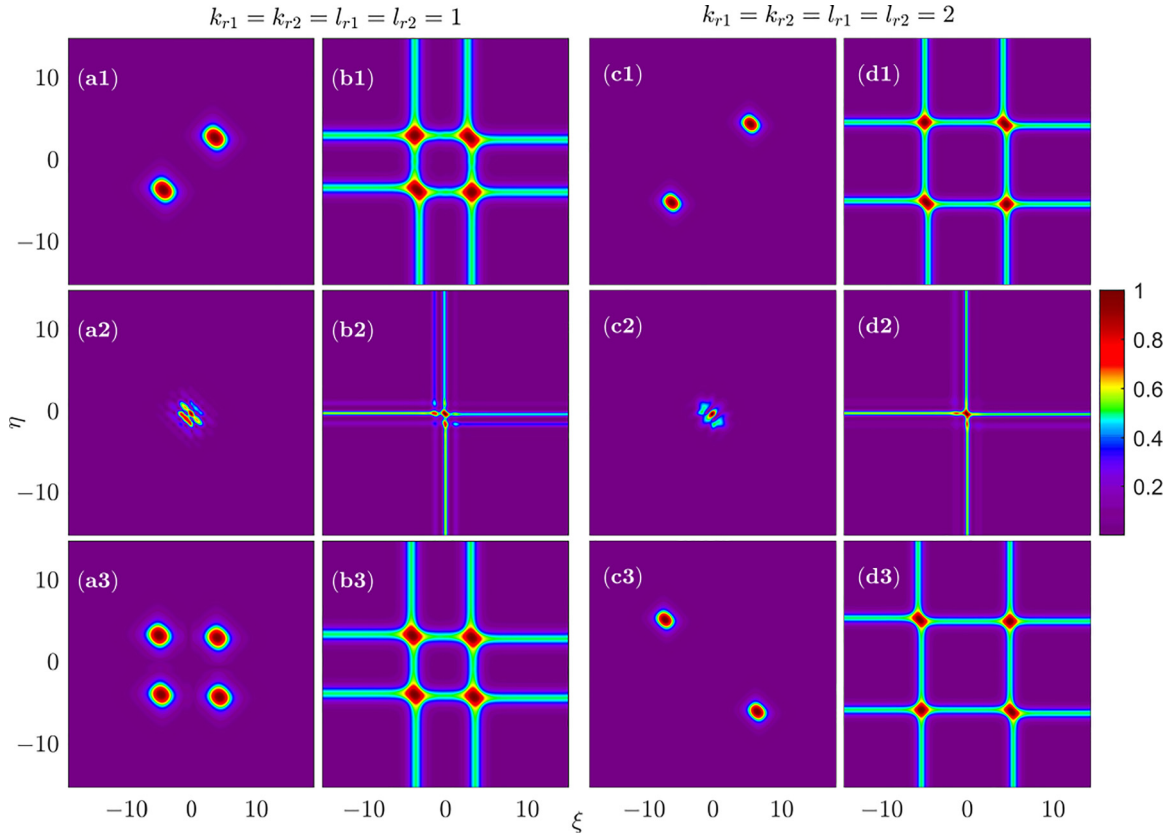


FIG. 5. Collision between two matter-wave dromions, with  $k_{i1} = k_{i2} = -l_{i1} = -l_{i2} = 2$ ,  $\gamma_1 = 3$ ,  $\gamma_2 = 3$ ,  $\phi_{\rho_1} = 0$ , and  $\phi_{\rho_2} = 0$ . (a1)–(a3) [(b1)–(b3)] Intensity profile of the short-wave component  $|A_1|^2$  (long-wave component  $|A_0|^2$ ) for  $k_{r1} = k_{r2} = l_{r1} = l_{r2} = 1$ , which are taken to be functions of  $\xi$  and  $\eta$  for  $\tau = 0, 1, 3$ , respectively. The collision between two dromions is inelastic. (c1)–(c3) [(d1)–(d3)] Intensity profile of the short-wave component  $|A_1|^2$  (long-wave component  $|A_0|^2$ ) for  $k_{r1} = k_{r2} = l_{r1} = l_{r2} = 2$ , which are taken to be functions of  $\xi$  and  $\eta$  for  $\tau = 0, 1, 3$ , respectively. The collision between two dromions is elastic.

numerical simulation on the DS equations (9a) and (9b), by adding 10% noise into the initial condition of the dromion. Shown in Fig. 4 are intensity distributions of the short-wave component  $|A_1|^2$  [Figs. 4(a1)–4(c1)] and the long-wave component  $|A_0|^2$  [Figs. 4(a2)–4(c2)] of the dromion, which are taken to be functions of  $\xi$  and  $\eta$ , for the dimensionless time  $\tau = 0, 1, 2$ , respectively. One sees that the dromion is quite stable during propagation.

In passing, we indicated that it is possible to experimentally observe the matter-wave dromion predicted here by using a Bose-condensed atomic gas with dipole-dipole interaction (such as  $^{164}\text{Dy}$  [24]), confined in a disk-shaped trap. By setting the system parameters described at the beginning of Sec. III A, one can realize the condition of repulsive interaction. Then, by making the system work at the modulationally stable region of the ground-state background, and using an initial excitation prepared by an imprinting technique [5], one can excited the dromion in the disk-shaped dipolar BEC and observe its propagation in the system.

#### IV. COLLISION, REFLECTION, AND TRANSMISSION OF THE MATTER-WAVE DROMIONS

##### A. Collision between two dromions

To have a further understanding on the physical property of the matter-wave dromions described above, it is of interest to explore their behaviors of collision, reflection, and transmission. To investigate the interaction between dromions, we assume that the initial condition of the system is a superposition of two dromion solutions, each of which has the form of (11), i.e.,  $u|_{t=0} = \sum_{j=1}^2 \varrho/F[\eta_1(x' + d_j, y' + d_j), \eta_2(x' + d_j, y' + d_j)] \exp[\eta_1(x' + d_j, y' + d_j) + \eta_2(x' + d_j, y' + d_j)]$ . Here the parameters are chosen to be  $k_{i1} = k_{i2} = -l_{i1} = -l_{i2} = 2$ ,  $\gamma_1 = \gamma_2 = 3$ ,  $\phi_{\rho_1} = 0$ , and  $\phi_{\rho_2} = 0$ ; in addition, we choose  $d_1 = -4$  and  $d_2 = 4$ , which describe the positions of the first and second dromions, respectively. With the function  $F$  given here, the initial condition for  $s|_{t=0}$  can be obtained by the second expression of (11).

Shown in Fig. 5 is the result of the collision between the two dromions through numerically solving the DS equations (9a) and (9b) in the presence of the LHY correction. Figures 5(a1)–5(a3) illustrate the intensity profile of the short-wave component  $|A_1|^2$  (before, during, and after the collision) for  $k_{r1} = k_{r2} = l_{r1} = l_{r2} = 1$ , by taking it as a function of  $\xi$  and  $\eta$  for  $\tau = 0, 1, 3$ , respectively; Figs. 5(b1)–5(b3) show the corresponding result for the long-wave component  $|A_0|^2$ . We see that, after the collision, though the long-wave component  $|A_0|^2$  can keep its shape nearly invariant, the short-wave component  $|A_1|^2$  is split into four parts. Thus in this case the collision between the two dromions is inelastic. The physical reason for the occurrence of such an inelastic collision is the following. Since  $k_{rj}$  and  $l_{rj}$  ( $j = 1, 2$ ) are small, each part of the short-wave component  $|A_1|^2$  has a large spatial width, and hence the diffraction effect is weak and cannot balance the nonlinear effect in the system. In addition, the long-wave component  $|A_0|^2$  (formed by the intersection of the four antikinks) provides an attractive force to the short-wave component  $|A_1|^2$ . At the four intersections of  $|A_0|^2$ , the attractive force is strongest, which focuses the energy of  $|A_1|^2$

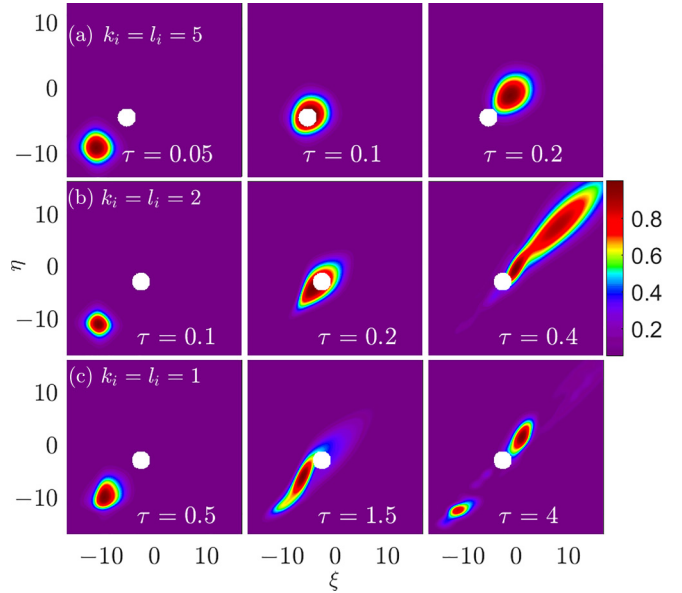


FIG. 6. Matter-wave dromion scattered by an obstacle (denoted by the white circle). (a)  $k_i = l_i = 5$ : the dromion passes the obstacle without large deformation for large incident velocity. (b)  $k_i = l_i = 2$ : the dromion can pass the obstacle but with drastic deformation for intermediate incident velocity. (c)  $k_i = l_i = 1$ : the dromion is partially reflected and partially transmitted after being scattered by the obstacle for smaller incident velocity.

into the four intersections and thus results in the appearance of four pulses in the distribution of  $|A_1|^2$ .

Nevertheless, if  $k_{rj}$  and  $l_{rj}$  ( $j = 1, 2$ ) are increased, the outcome of the two-dromion collision will be changed drastically. Shown in Figs. 5(c1)–5(c3) are the intensity profiles of  $|A_1|^2$  for  $k_{r1} = k_{r2} = l_{r1} = l_{r2} = 2$ , by taking it also as a function of  $\xi$  and  $\eta$  for  $\tau = 0, 1, 3$ , respectively; Figs. 5(d1)–5(d3) give the corresponding result of  $|A_0|^2$ . One sees that, in this situation, the collision between the two dromions is very robust and hence can be taken as an elastic one. The reason is that, for larger  $k_{rj}$  and larger  $l_{rj}$ , each part of the short-wave component  $|A_1|^2$  has a smaller spatial width, and the diffraction effect is increased and can balance the nonlinear effect in the system. Thereby, the two pulses of  $|A_1|^2$  can keep their wave shapes after their collision. However, the propagation directions of the two pulses are changed after the collision.

##### B. Reflection and transmission of dromions scattered by impurities

Finally, we investigate reflection and transmission behaviors of the dromion numerically when it is scattered by an impurity. In the simulation, we assume that the impurity can be described by a repulsive Gaussian potential with the form  $V = V_0 \exp[-(\xi^2 + \eta^2)/4]$ , with parameters given by  $V_0 = 3$ . Shown in Fig. 6 are numerical results of the scattering by the obstacle (denoted by the white circles) for different incident velocities of the dromion, controlled by the parameter  $k_i$  and  $l_i$  in the approximated solution (11).

Figure 6(a) shows the case of the dromion before (the left panel), during (the central panel), and after (the right panel) passing the obstacle, with a large incident velocity (i.e.,

$k_i = l_i = 5$ ). We see that the dromion is rather robust, i.e., it can pass the obstacle without large deformation. For an intermediate incident velocity ( $k_i = l_i = 2$ ), the dromion can pass the obstacle, but with a drastic deformation and a very small reflection, which is illustrated in Fig. 6(b). However, for a small incident velocity ( $k_i = l_i = 1$ ), the dromion is partially reflected and partially transmitted after being scattered by the obstacle; see the result given by Fig. 6(c).

## V. DISCUSSION AND SUMMARY

The asymptotic reduction used in Sec. III A for deriving the DS equations (9a) and (9b) requires that the Fourier transform of  $U_{dd}$  exists, which is the case for the dipole-dipole interaction considered here. We stress that such an asymptotic reduction is one of the examples for general processes, and it can be generalized to other types of atom-atom interactions as long as the Fourier transform of the kernel  $U_{dd}$  exists.

The above analysis shows that the DS equations (9a) and (9b) describing the weak nonlinear matter-wave excitations can be simplified into DSI equations. Since in high-dimensional soliton theory DSII equations are also of much interest [29], one may ask the question whether or not the DSII equations can be obtained in the present dipolar BEC. However, after analyzing possible parameter domains, we find that amplitude equations for the system under our consideration here cannot be reduced into the DSII equations.

On the other hand, the LHY correction can be very different depending on the relevant settings and space dimensionality. It can be cubic, quadratic [48], or a complicated logarithm form [49]. Here we consider the simple cubic form, which is obtained by using a local density approximation in three-dimensional space. An application of our paper to cases

with different LHY correction terms will be interesting but is beyond the scope of the present paper.

In conclusion, in this paper we have investigated the weak nonlinear dynamics of (2+1)D matter waves in a disk-shaped dipolar BEC when quantum fluctuations are taken into account. By applying the method of multiple scales, we have derived the DSI equations governing the nonlinear evolution of matter-wave envelopes. We have shown that the system supports (2+1)D matter-wave dromions, which are superpositions of short-wavelength excitation and long-wavelength mean flow. We have found that the stability of the matter-wave dromions can be largely enhanced by the quantum fluctuations described by the LHY correction. We have also found that such dromions possess many interesting characters for collision, reflection, and transmission when they interact with each other and are scattered by obstacles. The results reported here are beneficial not only for understanding the physical property of the quantum fluctuations in BECs, but also for finding new nonlinear localized excitations in systems with long-ranged interactions experimentally.

## ACKNOWLEDGMENT

This work was supported by the National Natural Science Foundation of China under Grant No. 11975098 and Hubei University of Automotive Technology under Grant No. BK202210.

## APPENDIX A: DERIVATION OF THE AMPLITUDE EQUATIONS

In this Appendix, we give the detailed derivation of the amplitude equations based on the following equation:

$$i \frac{\partial \varphi(\vec{\rho}, t_1)}{\partial t_1} = \left[ -\frac{1}{2} \bar{\nabla}_\perp^2 + \int d\vec{\xi} R(\vec{\xi} - \vec{\xi}') |\varphi(\vec{\rho}')|^2 + w_2 |\varphi|^3 \right] \varphi, \quad (\text{A1})$$

where  $\vec{\rho} = (x_1, y_1)$ ,  $R(\vec{\rho}) = gU_{2D}(\vec{\rho}) + w_1 \delta(\vec{\rho})$  with  $w_1$ ,  $w_2$ , and  $g$  characterizing the contact interaction, quantum fluctuations, and the dipole-dipole interaction. Letting  $\varphi(\vec{\rho}, t_1) = P(\vec{\rho}, t_1) \exp[-i\mu t_1 + i\tilde{\varphi}(\vec{\rho}, t_1)]$ , with  $\mu = u_0^2 \hat{K}(0) + w_2 u_0^3$  and  $u_0$  a constant, we obtain

$$\frac{\partial P}{\partial t_1} + \nabla P \cdot \nabla \tilde{\varphi} + \frac{1}{2} \nabla^2 \tilde{\varphi} = 0, \quad (\text{A2a})$$

$$P \frac{\partial \tilde{\varphi}}{\partial t_1} - \frac{1}{2} \nabla^2 P - \mu P + \frac{1}{2} P |\nabla \tilde{\varphi}|^2 + w_2 P^4 + P \int R(\vec{\rho} - \vec{\rho}') P^2(\vec{\rho}') d^2 \vec{\rho}' = 0. \quad (\text{A2b})$$

Following the idea of the method of multiple scales [36], we make the asymptotic expansion  $P = u_0 + \epsilon a_1 + \epsilon^2 a_2 + \epsilon^3 a_3$  and  $\tilde{\varphi} = \epsilon \phi_1 + \epsilon^2 \phi_2 + \epsilon^3 \phi_3$ . Those variables are the functions of  $\theta = \beta x_1 - \omega t_1$ ,  $\tau = \epsilon^2 t_1$ ,  $\xi = \epsilon(x_1/v_g - t_1)$ , and  $\eta = \epsilon y_1$ . Thus we have  $\frac{\partial}{\partial x_1} = \beta \frac{\partial}{\partial \theta} + \epsilon \frac{1}{v_g} \frac{\partial}{\partial \xi}$ ,  $\frac{\partial}{\partial y_1} = \epsilon \frac{\partial}{\partial \eta}$ , and  $\frac{\partial}{\partial t_1} = -\omega \frac{\partial}{\partial \theta} - \epsilon \frac{\partial}{\partial \xi} + \epsilon^2 \frac{\partial}{\partial \tau}$ . Substituting the above expansion into Eqs. (A2a) and (A2b), we obtain

$$-\omega \frac{\partial a_j}{\partial \theta} + \frac{1}{2} u_0 \beta^2 \frac{\partial^2 \phi_j}{\partial \theta^2} = \alpha_j, \quad (\text{A3a})$$

$$-\frac{1}{2} \beta^2 \frac{\partial^2 a_j}{\partial \theta^2} + 2u_0^2 \int R(\vec{\xi}') a_j d\vec{\xi} - \omega u_0 \frac{\partial \phi_j}{\partial \theta} + 3W_2 u_0^3 a_j = \beta_j, \quad (\text{A3b})$$

$j = 1, 2, 3, \dots$ . By eliminating  $a_j$ , we get the closed equation for  $\phi_j$ :

$$-\frac{1}{4} \beta^4 \frac{\partial^4 \phi_j}{\partial \theta^4} + \left( \frac{3}{2} W_2 u_0^3 \beta^2 - \omega^2 \right) \frac{\partial^2 \phi_j}{\partial \theta^2} + u_0^2 \beta^2 \int R(\vec{\xi}) \frac{\partial^2 \phi_j}{\partial \theta^2} d\vec{\xi} = 2u_0 \int R(\vec{\xi}) \alpha_j d\vec{\xi} + 3W_2 u_0^2 \alpha_j + \frac{\omega}{u_0} \frac{\partial \beta_j}{\partial \theta} - \frac{\beta^2}{2u_0} \frac{\partial^2 \alpha_j}{\partial \theta^2}. \quad (\text{A4})$$

The expressions for  $\alpha_j$  and  $\beta_j$  are respectively given by

$$\alpha_1 = 0, \quad \beta_1 = 0, \quad (\text{A5a})$$

$$\alpha_2 = \frac{\partial a_1}{\partial \xi} - \beta^2 \frac{\partial a_1}{\partial \theta} \frac{\partial \phi_1}{\partial \theta} - \frac{u_0 \beta}{v_g} \frac{\partial^2 \phi_1}{\partial \theta \partial \xi} - \frac{1}{2} \beta^2 a_1 \frac{\partial^2 \phi_1}{\partial \theta^2}, \quad (\text{A5b})$$

$$\begin{aligned} \beta_2 = & \frac{\beta}{v_g} \frac{\partial^2 a_1}{\partial \theta \partial \xi} + u_0 \frac{\partial \phi_1}{\partial \xi} + \omega a_1 \frac{\partial \phi_1}{\partial \theta} - \frac{1}{2} u_0 \beta^2 \left( \frac{\partial \phi_1}{\partial \theta} \right)^2 - 2u_0 \int R(\vec{\zeta}) a_1 d\vec{\zeta} a_1 - 2u_0^2 \int R(\vec{\zeta}) \left( w_1 \frac{\partial a_1}{\partial \xi} + w_2 \frac{\partial a_1}{\partial \eta} \right) d\vec{\zeta} \\ & - u_0 \int R(\vec{\zeta}) a_1^2 d\vec{\zeta} - 6W_2 u_0^2 a_1^2, \end{aligned} \quad (\text{A5c})$$

$$\begin{aligned} \alpha_3 = & \frac{\partial a_2}{\partial \xi} - \frac{\partial a_1}{\partial \tau} - \beta \frac{\partial a_1}{\partial \theta} \left( \beta \frac{\partial \phi_2}{\partial \theta} + \frac{1}{v_g} \frac{\partial \phi_1}{\partial \xi} \right) - \frac{1}{2} \beta^2 a_2 \frac{\partial^2 \phi_1}{\partial \theta^2} - \beta \frac{\partial \phi_1}{\partial \theta} \left( \beta \frac{\partial a_2}{\partial \theta} + \frac{1}{v_g} \frac{\partial a_1}{\partial \xi} \right) - \frac{u_0 \beta}{v_g} \frac{\partial^2 \phi_2}{\partial \theta \partial \xi} - \frac{1}{2} u_0 \frac{\partial^2 \phi_1}{\partial \eta^2} \\ & - \frac{u_0}{2v_g^2} \frac{\partial^2 \phi_1}{\partial \xi^2} - \frac{1}{2} a_1 \left( \beta^2 \frac{\partial^2 \phi_2}{\partial \theta^2} + \frac{2\beta}{v_g} \frac{\partial^2 \phi_1}{\partial \theta \partial \xi} \right), \end{aligned} \quad (\text{A6a})$$

$$\begin{aligned} \beta_3 = & \omega a_2 \frac{\partial \phi_1}{\partial \theta} + a_1 \left( \omega \frac{\partial \phi_2}{\partial \theta} + \frac{\partial \phi_1}{\partial \xi} \right) + u_0 \left( \frac{\partial \phi_2}{\partial \xi} - \frac{\partial \phi_1}{\partial \tau} \right) + \frac{1}{2} \frac{\partial^2 a_1}{\partial \eta^2} + \frac{\beta}{v_g} \frac{\partial^2 a_2}{\partial \theta \partial \xi} + \frac{1}{2v_g^2} \frac{\partial^2 a_1}{\partial \xi^2} - \frac{1}{2} \beta^2 a_1 \left( \frac{\partial \phi_1}{\partial \theta} \right)^2 \\ & - u_0 \beta^2 \frac{\partial \phi_1}{\partial \theta} \frac{\partial \phi_2}{\partial \theta} - \frac{u_0 \beta}{v_g} \frac{\partial \phi_1}{\partial \theta} \frac{\partial \phi_1}{\partial \xi} - 4W_2 (u_0 a_1^3 + 3u_0^2 a_1 a_2) - 2u_0 \int R(\vec{\zeta}) a_1 d\vec{\zeta} a_2 - 2u_0 \int R(\vec{\zeta}) a_1 a_2 d\vec{\zeta} \\ & - a_1 \int R(\vec{\zeta}) \left[ 2u_0 \left( w_1 \frac{\partial a_1}{\partial \xi} + w_2 \frac{\partial a_1}{\partial \eta} + a_2 \right) + a_1^2 \right] d\vec{\zeta} - u_0^2 \int R(\vec{\zeta}) \left[ w_1^2 \frac{\partial^2 a_1}{\partial \xi^2} + w_2^2 \frac{\partial^2 a_1}{\partial \eta^2} + 2w_1 w_2 \frac{\partial^2 a_1}{\partial \xi \partial \eta} \right. \\ & \left. + 2w_1 \frac{\partial a_2}{\partial \xi} + 2w_2 \frac{\partial a_2}{\partial \eta} \right] d\vec{\zeta}. \end{aligned} \quad (\text{A6b})$$

### 1. First-order solution

We now solve Eq. (A4) order by order. At the first-order approximation ( $j = 1$ ), we have the equation

$$-\frac{1}{4} \beta^4 \frac{\partial^4 \phi_1}{\partial \theta^4} + b \frac{\partial^2 \phi_1}{\partial \theta^2} + u_0^2 \beta^2 \int R(\vec{\zeta}) \frac{\partial^2 \phi_1}{\partial \theta^2} d\vec{\zeta} = 0, \quad (\text{A7})$$

where  $b = \frac{3}{2} W_2 u_0^3 \beta^2 - \omega^2$ . Its solution is of the form

$$\phi_1 = A_0 + A_1 e^{i\theta} + \bar{A}_1 e^{-i\theta}, \quad (\text{A8})$$

where  $A_0$  and  $A_1$  are, respectively, the amplitude (envelope) of the short-wave and that of the long-wave (mean flow) component, both of which are functions of the slow variables  $\xi$ ,  $\eta$ , and  $\tau$ , yet to be determined. The solution of  $a_1$  reads

$$a_1 = i \frac{u_0 \beta^2}{2\omega} A_1 e^{i\theta} - i \frac{u_0 \beta^2}{2\omega} \bar{A}_1 e^{-i\theta} \equiv i c_1 A_1 e^{i\theta} + \text{c.c.} \quad (\text{A9})$$

Here, the linear dispersion relation is given by

$$\omega = \omega(\beta) \equiv \left[ \frac{1}{4} \beta^4 + u_0^2 \beta^2 \hat{R}(\beta) + \frac{3}{2} w_2 u_0^3 \beta^2 \right]^{1/2}, \quad (\text{A10})$$

with  $\hat{R}(\beta)$  being the Fourier transform of  $R(\vec{\rho}) \equiv gU_{2D}(\vec{\rho}) + w_1 \delta(\vec{\rho})$ .

### 2. Second-order solution

At the second-order approximation ( $j = 2$ ), by substituting the above first-order solution into Eqs. (A5b) and (A5c) we get

$$\alpha_2 = i \left( c_1 - \frac{\beta u_0}{v_g} \right) \left( \frac{\partial A_1}{\partial \xi} e^{i\theta} - \frac{\partial \bar{A}_1}{\partial \xi} e^{-i\theta} \right) + \frac{3}{2} i c_1 \beta^2 (A_1^2 e^{2i\theta} - \bar{A}_1^2 e^{-2i\theta}), \quad (\text{A11a})$$

$$\begin{aligned} \beta_2 = & \left( u_0 - \frac{c_1 \beta}{v_g} - \frac{2c_1 u_0^2}{v_g} \frac{d\hat{R}(\beta)}{d\beta} \right) \left( \frac{\partial A_1}{\partial \xi} e^{i\theta} + \frac{\partial \bar{A}_1}{\partial \xi} e^{-i\theta} \right) + (6u_0^2 W_2 + 2u_0 \hat{R}(\beta) + u_0 \hat{R}(2\beta)) c_1^2 (A_1^2 e^{2i\theta} + \bar{A}_1^2 e^{-2i\theta}) \\ & - (12u_0^2 W_2 + 4u_0 \hat{R}(\beta) + 2u_0 \hat{R}(0)) c_1^2 |A_1|^2 + u_0 \frac{\partial A_0}{\partial \xi} \\ \equiv & \beta_{21} \left( \frac{\partial A_1}{\partial \xi} e^{i\theta} + \frac{\partial \bar{A}_1}{\partial \xi} e^{-i\theta} \right) + \beta_{22} (A_1^2 e^{2i\theta} + \bar{A}_1^2 e^{-2i\theta}) + \beta_{23} |A_1|^2 + u_0 \frac{\partial A_0}{\partial \xi} \end{aligned} \quad (\text{A11b})$$

where  $\hat{R}(\beta)$  is the Fourier transform of  $R(\bar{\rho})$ . Then the right-hand side of Eq. (A4) reads

$$\mathcal{L}_2 = il_{21} \frac{\partial A_1}{\partial \xi} e^{i\theta} - il_{21} \frac{\partial \bar{A}_1}{\partial \xi} e^{-i\theta} + il_{22} A_1^2 e^{2i\theta} - il_{22} \bar{A}_1^2 e^{-2i\theta}, \tag{A12}$$

where  $l_{22} = 3c_1\beta^4/u_0 + 3u_0c_1\beta^2\hat{R}(2\beta) + \frac{9}{2}u_0^2c_1\beta^2W_2 + 2\omega\beta_{22}/u_0$ . The solvability condition needs  $l_{21} = 0$ , and we hence have  $v_g = \frac{1}{2\omega}[\beta^3 + 2u_0\beta\hat{R}(\beta) + 3u_0^3W_2\beta + u_0^2\beta^2\frac{d\hat{R}(\beta)}{d\beta}]$ . Therefore, the solutions of  $\phi_2$  and  $a_2$  are given by

$$\phi_2 = -\frac{il_{22}(A_1^2 e^{2i\theta} - \bar{A}_1^2 e^{-2i\theta})}{4\beta^4 + 6W_2u_0^3\beta^2 + 4u_0^2\beta^2\hat{R}(2\beta) - 4\omega^2}, \tag{A13}$$

$$a_2 = a_{20}|A_1|^2 + a_{21} \frac{\partial A_0}{\partial \xi} + \left[ a_{22} \frac{\partial A_1}{\partial \xi} e^{i\theta} + a_{23} A_1^2 e^{2i\theta} + \text{c.c.} \right], \tag{A14}$$

where  $a_{20} = \frac{\beta_{23}}{2u_0^2\hat{R}(0)+3W_2u_0^3}$ ,  $a_{21} = \frac{u_0}{2u_0^2\hat{R}(0)+3W_2u_0^3}$ ,  $a_{22} = \frac{1}{\omega}(\frac{u_0\beta}{v_g} - c_1) \equiv \frac{u_0\beta}{2\omega^3v_g}[u_0^2\beta^2\hat{R}(\beta) + \frac{3}{2}u_0^2W_2\beta^2 - \frac{1}{2}u_0^2\beta^3\frac{d\hat{R}(\beta)}{d\beta}]$ ,  $m = -\frac{il_{22}}{4\beta^4+6W_2u_0^3\beta^2+4u_0^2\beta^2\hat{R}(2\beta)-4\omega^2}$ , and  $a_{23} = -\frac{\beta^2}{\omega}(u_0m + \frac{3}{4}c_1)$ .

### 3. Third-order solution

At the third-order approximation ( $j = 3$ ), by substituting the above first- and second-order solutions into Eqs. (A6a) and (A6b) we have

$$\alpha_3 = \left( a_{21} - \frac{u_0}{2v_g^2} \right) \frac{\partial^2 A_0}{\partial \xi^2} - \frac{u_0}{2} \frac{\partial^2 A_0}{\partial \eta^2} + \left( a_{20} - \frac{1}{2}\beta^2 a_{22} - \frac{\beta c_1}{v_g} \right) \frac{\partial |A_1|^2}{\partial \xi} + \left[ -ic_1 \frac{\partial A_1}{\partial \tau} - \frac{1}{2}u_0 \frac{\partial^2 A_1}{\partial \eta^2} + \frac{1}{2}(a_{20} - 3a_{23})\beta^2 |A_1|^2 A_1 + \left( \frac{1}{2}a_{21}\beta^2 + \frac{c_1\beta}{v_g} \right) A_1 \frac{\partial A_0}{\partial \xi} + \left( a_{22} - \frac{u_0}{2v_g^2} \right) \frac{\partial^2 A_1}{\partial \xi^2} \right] e^{i\theta} + (\cdot)e^{2i\theta} + \text{c.c.}, \tag{A15a}$$

$$\beta_3 = \left[ \frac{ic_1}{2} \frac{\partial^2 A_1}{\partial \eta^2} - u_0 \frac{\partial A_1}{\partial \tau} + iH_1 A_1 \frac{\partial A_0}{\partial \xi} + iH_2 \frac{\partial^2 A_1}{\partial \xi^2} + iH_3 |A_1|^2 A_1 \right] e^{i\theta} + (\cdot)e^{2i\theta} + \text{c.c.}, \tag{A15b}$$

where  $H_1 = c_1 - 12a_{21}c_1u_0^2W_2 + a_{21}\omega - \frac{\beta u_0}{v_g} + 2c_1u_0a_{21}[\hat{R}(0) - 2\hat{R}(\beta)]$ ,  $H_2 = \frac{c_1}{2v_g^2} + \frac{a_{22}\beta}{v_g} + u_0^2c_1\frac{d^2\hat{R}(\beta)}{d\beta^2} + u_0^2a_{22}\frac{d\hat{R}(\beta)}{d\beta}$ ,  $H_3 = 12W_2u_0c_1(a_{23}u_0 - a_{20}u_0 - c_1^2) + (a_{20} - a_{23})\omega - \frac{3c_1\beta^2}{2} + 2c_1m\omega - 2\beta^2mu_0 + 4c_1u_0\hat{R}(\beta)(a_{23} - a_{20}) + 2u_0c_1a_{23}\hat{R}(2\beta) + 2c_1u_0a_{20}\hat{R}(0) + c_1^3[2\hat{R}(0) - \hat{R}(2\beta)]$ . The right-hand side of Eq. (A4) reads

$$\mathcal{L}_3 = [2u_0\hat{R}(0) + 2W_2u_0^2] \left[ \left( a_{21} - \frac{u_0}{2v_g^2} \right) \frac{\partial^2 A_0}{\partial \xi^2} - \frac{u_0}{2} \frac{\partial^2 A_0}{\partial \eta^2} + \left( a_{20} - \frac{1}{2}\beta^2 a_{22} - \frac{\beta c_1}{v_g} \right) \frac{\partial |A_1|^2}{\partial \xi} \right] + \left\{ -2i\omega \frac{\partial A_1}{\partial \tau} - \left( \frac{\omega^2}{\beta^2} + \frac{\beta^2}{4} \right) \frac{\partial^2 A_1}{\partial \eta^2} + \left[ \frac{2\omega^2}{u_0\beta^2} \left( a_{22} - \frac{u_0}{2v_g^2} \right) - \frac{\omega}{u_0} H_2 \right] \frac{\partial^2 A_1}{\partial \xi^2} + \left( \frac{\omega^2}{u_0} (a_{20} - 3a_{23}) - \frac{\omega}{u_0} H_3 \right) |A_1|^2 A_1 + \left[ \frac{2\omega^2}{u_0\beta^2} \left( \frac{a_{21}}{2}\beta^2 + \frac{c_1\beta}{v_g} \right) - \frac{\omega}{u_0} H_1 \right] A_1 \frac{\partial A_0}{\partial \xi} \right\} e^{i\theta}. \tag{A16}$$

The solvability condition at this order gives the equations for  $A_0$  and  $A_1$ :

$$\left( a_{21} - \frac{u_0}{2v_g^2} \right) \frac{\partial^2 A_0}{\partial \xi^2} - \frac{u_0}{2} \frac{\partial^2 A_0}{\partial \eta^2} + \left( a_{20} - \frac{1}{2}\beta^2 a_{22} - \frac{\beta c_1}{v_g} \right) \frac{\partial |A_1|^2}{\partial \xi} = 0, \tag{A17a}$$

$$-2i\omega \frac{\partial A_1}{\partial \tau} - \left( \frac{\omega^2}{\beta^2} + \frac{\beta^2}{4} \right) \frac{\partial^2 A_1}{\partial \eta^2} + K_1 \frac{\partial^2 A_1}{\partial \xi^2} + W_1 |A_1|^2 A_1 + \left[ \frac{2\omega^2}{u_0\beta^2} \left( \frac{a_{21}}{2}\beta^2 + \frac{c_1\beta}{v_g} \right) - \frac{\omega}{u_0} H_1 \right] A_1 \frac{\partial A_0}{\partial \xi} = 0 \tag{A17b}$$

where  $K_1 = [\frac{2\omega^2}{u_0\beta^2} (a_{22} - \frac{u_0}{2v_g^2}) - \frac{\omega}{u_0} H_2]$  and  $W_1 = (\frac{\omega^2}{u_0} (a_{20} - 3a_{23}) - \frac{\omega}{u_0} H_3)$ . After simplification, the above equations become

$$\alpha_1 \frac{\partial^2 A_0}{\partial \xi^2} - \frac{\partial^2 A_0}{\partial \eta^2} + \alpha_2 \frac{\partial |A_1|^2}{\partial \xi} = 0, \tag{A18a}$$

$$i \frac{\partial A_1}{\partial \tau} + \delta_1 \frac{\partial^2 A_1}{\partial \xi^2} + \delta_2 \frac{\partial^2 A_1}{\partial \eta^2} + \delta_3 |A_1|^2 A_1 + \delta_4 A_1 \frac{\partial A_0}{\partial \xi} = 0, \tag{A18b}$$

where

$$\alpha_1 = \frac{2a_{21}}{u_0} - \frac{1}{v_g^2} \equiv \frac{2}{2u_0^2\hat{R}(0) + 3W_2u_0^3} - \frac{1}{v_g^2}, \quad (\text{A19a})$$

$$\alpha_2 = \frac{2}{u_0} \left( a_{20} - \frac{1}{2}\beta^2 a_{22} - \frac{\beta c_1}{v_g} \right), \quad (\text{A19b})$$

$$\delta_1 = -\frac{1}{2\omega} \left[ \frac{2\omega^2}{u_0\beta^2} \left( a_{22} - \frac{u_0}{2v_g^2} \right) - \frac{\omega}{u_0} H_2 \right], \quad (\text{A19c})$$

$$\delta_2 = \frac{1}{2\omega} \left( \frac{\omega^2}{\beta^2} + \frac{\beta^2}{4} \right), \quad (\text{A19d})$$

$$\delta_3 = -\frac{1}{2\omega} \left( \frac{\omega^2}{u_0} (a_{20} - 3a_{23}) - \frac{\omega}{u_0} H_3 \right), \quad (\text{A19e})$$

$$\delta_4 = -\frac{1}{2\omega} \left[ \frac{2\omega^2}{u_0\beta^2} \left( \frac{a_{21}}{2}\beta^2 + \frac{c_1\beta}{v_g} \right) - \frac{\omega}{u_0} H_1 \right]. \quad (\text{A19f})$$

## APPENDIX B: MODULATION INSTABILITY

The plane-wave (i.e., ground state of the BEC) solution of Eq. (4) for  $V_0 = 0$  reads

$$\varphi(\vec{\rho}, t_1) = u_0 e^{-i\mu t_1}, \quad (\text{B1})$$

with  $\mu = u_0^2[w_1 + u_0 w_2 + g \iint U_{2D}(\vec{\zeta}) d^2\zeta]$  and  $u_0 = 1/(\iint d^2\zeta)^{1/2}$ . The MI of this plane-wave solution can be analyzed by assuming

$$\tilde{\varphi}(\vec{\rho}, t_1) = [u_0 + a_1 e^{i\vec{\beta}\cdot\vec{\rho} + \sigma t_1} + a_2^* e^{-i\vec{\beta}\cdot\vec{\rho} + \sigma^* t_1}] e^{-i\mu t_1}, \quad (\text{B2})$$

where  $a_1$  and  $a_2$  are small complex amplitudes characterizing the perturbation to the ground state,  $\vec{\beta} = (\beta_1, \beta_2)$  is the wave vector of the perturbation in the  $x_1$ - $y_1$  plane, and  $\sigma$  is the growth rate of the perturbation.

Substituting (B2) into Eq. (4) and keeping only linear terms of  $a_1$  and  $a_2$ , we get the expression of the growth rate:

$$\sigma^2 = -\beta^2 \left[ \frac{1}{4}\beta^2 + \frac{3}{2}u_0^3 w_2 + u_0^2 w_1 + g u_0^2 \mathcal{U}_{2D}(\vec{\beta}) \right], \quad (\text{B3})$$

with

$$\mathcal{U}_{2D}(\vec{\beta}) = \frac{2\sqrt{2\pi}}{3} [F_{\parallel}(\vec{\beta}/\sqrt{2}) \sin^2(\alpha) + F_{\perp}(\vec{\beta}/\sqrt{2}) \cos^2(\alpha)]. \quad (\text{B4})$$

Here  $\beta = \sqrt{\beta_1^2 + \beta_2^2}$ ,  $F_{\parallel}(\vec{\beta}) = 3\sqrt{\pi}\beta_1^2 \exp(\beta^2) \text{erfc}(\beta)/\beta - 1$ , and  $F_{\perp}(\vec{\beta}) = 2 - 3\sqrt{\pi}\beta \exp(\beta^2) \text{erfc}(\beta)$ , with  $\text{erfc}$  the complementary error function. For  $\alpha = 0$ , the growth rate  $\sigma$  is independent of the propagation direction of the perturbation,

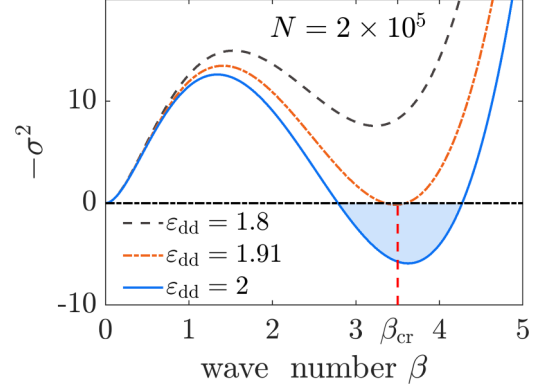


FIG. 7.  $-\sigma^2$  as a function of wave number  $\beta$  when  $N = 2 \times 10^5$ , for different relative dipolar strengths  $\varepsilon_{dd} \equiv a_{dd}/a_s = 1.8$  (dotted black line), 1.91 (dashed red line), and 2 (solid blue line), respectively. MI happens first at the critical wave number  $\beta_{cr} = 3.5$  when  $\varepsilon_{dd}$  reaches its threshold  $\varepsilon_{dd}^{cr} = 1.91$ .

while for  $\alpha \neq 0$ , it relies on the propagation direction and becomes anisotropic.

Using  $l_z = 45\pi a_{dd}$  and the relative dipolar strength  $\varepsilon_{dd} \equiv a_{dd}/a_s$ , (B3) becomes

$$\sigma^2 = -\beta^2 \left\{ \frac{1}{4}\beta^2 + \frac{2\sqrt{2\pi}}{45\pi} u_0^2 N \varepsilon_{dd}^{-1} + \frac{1}{15\pi} u_0^2 N \mathcal{U}_{2D}(\beta_1, \beta_2) + 64\sqrt{\frac{2}{5}} \pi^{-1/4} (45\pi)^{-5/2} \varepsilon_{dd}^{-5/2} \left[ 1 + \frac{3}{2} \varepsilon_{dd}^2 \right] u_0^3 N^{3/2} \right\}. \quad (\text{B5})$$

Shown in Fig. 7 is  $-\sigma^2$  as a function of the wave number  $\beta$  by taking  $N = 2 \times 10^5$ . The dotted black line, dashed red line, and solid blue line are ones for the relative dipolar strength  $\varepsilon_{dd} \equiv a_{dd}/a_s = 1.8, 1.91$ , and 2, respectively. One sees that the MI starts to occur at the critical wave number  $\beta = \beta_{cr} = 3.5$ , for which the corresponding threshold of the relative dipolar strength is given by  $\varepsilon_{dd} = \varepsilon_{dd}^{cr} = 1.91$ . The region with blue color in the figure is the one where MI appears.

Based on such calculations, the phase diagram for the existence and absence of MI in the  $N$ - $\varepsilon_{dd}$  plane can be obtained, as shown by Fig. 2(g) of the main text. In the region of modulational stability, the system supports the existence of matter-wave dromions, while in the region of modulational instability, the excitation in the system can undergo a spontaneous symmetry breaking and hence a self-organization into a supersolid crystal will occur [47], which is however a topic beyond the scope of the present paper.

- [1] L. Deng, E. Hagley, J. Wen, M. Trippenbach, Y. Band, P. S. Julienne, J. E. Simsarian, K. Helmerson, S. L. Rolston, and W. D. Phillips, Four-wave mixing with matter waves, *Nature (London)* **398**, 218 (1999).
- [2] S. Inouye, A. P. Chikkatur, D. M. Stamper-Kurn, J. Stenger, D. E. Pritchard, and W. Ketterle, Superradiant rayleigh scattering from a bose-einstein condensate, *Science* **285**, 571 (1999).

- [3] M. Kozuma, Y. Suzuki, Y. Torii, T. Sugiura, T. Kuga, E. W. Hagley, and L. Deng, Phase-Coherent amplification of matter waves, *Science* **286**, 2309 (1999).
- [4] E. A. Donley, N. R. Claussen, S. L. Cornish, J. L. Roberts, E. A. Cornell, and C. E. Wieman, Dynamics of collapsing and exploding Bose-Einstein condensates, *Nature (London)* **412**, 295 (2001).

- [5] J. Denschlag, J. E. Simsarian, D. L. Feder, C. W. Clark, L. A. Collins, J. Cubizolles, L. Deng, E. W. Hagley, K. Helmerson, W. P. Reinhardt, S. L. Rolston, B. I. Schneider, and W. D. Phillips, Generating solitons by phase engineering of a Bose-Einstein condensate, *Science* **287**, 97 (2000).
- [6] B. Eiermann, Th. Anker, M. Albiez, M. Taglieber, P. Treutlein, K.-P. Marzlin, and M. K. Oberthaler, Bright Bose-Einstein Gap Solitons of Atoms with Repulsive Interaction, *Phys. Rev. Lett.* **92**, 230401 (2004).
- [7] P. Meystre, *Atom Optics* (Springer, New York, 2001).
- [8] Y. S. Kivshar and G. P. Agrawal, *Optical Solitons: From Fibers to Photonic Crystals* (Academic Press, New York, 2003).
- [9] L. Khaykovich, F. Schreck, G. Ferrari, T. Bourdel, J. Cubizolles, L. D. Carr, and C. Salomon, Formation of a matter-wave bright soliton, *Science* **296**, 1290 (2002).
- [10] S. Burger, K. Bongs, S. Dettmer, W. Ertmer, K. Sengstock, A. Sanpera, G. V. Shlyapnikov, and M. Lewenstein, Dark Solitons in Bose-Einstein Condensates, *Phys. Rev. Lett.* **83**, 5198 (1999).
- [11] P. G. Kevrekidis, D. J. Frantzeskakis, and R. Carretero-González, *The Defocusing Nonlinear Schrödinger Equation: From Dark Soliton to Vortices and Vortex Rings* (SIAM, Philadelphia, 2015).
- [12] L. Pitaevskii and S. Stringari, *Bose-Einstein Condensation and Superfluidity* (Oxford University Press, New York, 2016).
- [13] P. Pedri and L. Santos, Two-Dimensional Bright Solitons in Dipolar Bose-Einstein Condensates, *Phys. Rev. Lett.* **95**, 200404 (2005).
- [14] I. Tikhonenkov, B. A. Malomed, and A. Vardi, Anisotropic Solitons in Dipolar Bose-Einstein Condensates, *Phys. Rev. Lett.* **100**, 090406 (2008).
- [15] R. Nath, P. Pedri, and L. Santos, Soliton-soliton scattering in dipolar Bose-Einstein condensates, *Phys. Rev. A* **76**, 013606 (2007).
- [16] M. Raghunandan, C. Mishra, K. Lakomy, P. Pedri, L. Santos, and R. Nath, Two-dimensional bright solitons in dipolar Bose-Einstein condensates with tilted dipoles, *Phys. Rev. A* **92**, 013637 (2015).
- [17] S. K. Adhikari, Stable, mobile, dark-in-bright, dipolar Bose-Einstein-condensate solitons, *Phys. Rev. A* **89**, 043615 (2014).
- [18] R. Nath, P. Pedri, and L. Santos, Stability of Dark Solitons in Three Dimensional Dipolar Bose-Einstein Condensates, *Phys. Rev. Lett.* **101**, 210402 (2008).
- [19] T. Bland, M. J. Edmonds, N. P. Proukakis, A. M. Martin, D. H. J. O'Dell, and N. G. Parker, Controllable nonlocal interactions between dark solitons in dipolar condensates, *Phys. Rev. A* **92**, 063601 (2015).
- [20] T. Lahaye, C. Menotti, L. Santos, M. Lewenstein, and T. Pfau, The physics of dipolar bosonic quantum gases, *Rep. Prog. Phys.* **72**, 126401 (2009).
- [21] D. Lee, K. Huang, and C. N. Yang, Eigenvalues and eigenfunctions of a Bose system of hard spheres and its low-temperature properties, *Phys. Rev.* **106**, 1135 (1957).
- [22] D. S. Petrov, Quantum Mechanical Stabilization of a Collapsing Bose-Bose Mixture, *Phys. Rev. Lett.* **115**, 155302 (2015).
- [23] B. A. Malomed, Vortex solitons: Old results and new perspectives, *Physica D* **399**, 108 (2019).
- [24] F. Böttcher, J.-N. Schmidt, J. Hertkorn, K. S. H. Ng, S. D. Graham, M. Guo, T. Langen, and T. Pfau, New states of matter with fine-tuned interactions: quantum droplets and dipolar supersolids, *Rep. Prog. Phys.* **84**, 012403 (2021).
- [25] Y.-C. Zhang, F. Maucher, and T. Pohl, Supersolidity around a Critical Point in Dipolar Bose-Einstein Condensates, *Phys. Rev. Lett.* **123**, 015301 (2019).
- [26] Y.-C. Zhang, T. Pohl, and F. Maucher, Phases of supersolids in confined dipolar Bose-Einstein condensates, *Phys. Rev. A* **104**, 013310 (2021).
- [27] J. Hertkorn, J.-N. Schmidt, M. Guo, F. Bottcher, K. S. H. Ng, S. D. Graham, P. Uerlings, T. Langen, M. Zwierlein, and T. Pfau, Pattern formation in quantum ferrofluids: From supersolids to superglasses, *Phys. Rev. Res.* **3**, 033125 (2021).
- [28] D. Edler, C. Mishra, F. Wächtler, R. Nath, S. Sinha, and L. Santos, Quantum Fluctuations in Quasi-One-Dimensional Dipolar Bose-Einstein Condensates, *Phys. Rev. Lett.* **119**, 050403 (2017).
- [29] M. J. Ablowitz and P. A. Clarkson, *Solitons, Nonlinear Evolution Equations and Inverse Scattering* (Cambridge University Press, Cambridge, England, 1991).
- [30] G. Huang, L. Deng, and C. Hang, Davey-Stewartson description of two-dimensional nonlinear excitations in Bose-Einstein condensates, *Phys. Rev. E* **72**, 036621 (2005).
- [31] Here “2” means two space dimensions, and “1” means the time dimension.
- [32] M. Boiti, J. J. P. Leon, L. M. Martina, and F. Pempinelli, Scattering of localized solitons in the plane, *Phys. Lett. A* **132**, 432 (1988).
- [33] A. S. Fokas and P. M. Santini, Dromions and a boundary value problem for the davey-stewartson i equation, *Physica D* **44**, 99 (1990).
- [34] W. Liu, Y. Zhang, Z. Luan, Q. Zhou, M. Mirzazadeh, M. Ekici, and A. Biswas, Dromion-like soliton interactions for nonlinear Schrodinger equation with variable coefficients in inhomogeneous optical fibers, *Nonlinear Dyn.* **96**, 729 (2019).
- [35] I. Ioannou-Sougleridis, D. J. Frantzeskakis, and T. P. Horikis, A Davey-Stewartson description of two-dimensional solitons in nonlocal media, *Stud. Appl. Math.* **144**, 3 (2020).
- [36] A. Jeffrey and T. Kawahara, *Asymptotic Methods in Nonlinear Wave Theory* (Pitman, London, 1982).
- [37] P. O. Fedichev, Y. Kagan, G. V. Shlyapnikov, and J. T. M. Walraven, Influence of Nearly Resonant Light on the Scattering Length in Low-Temperature Atomic Gases, *Phys. Rev. Lett.* **77**, 2913 (1996).
- [38] M. Theis, G. Thalhammer, K. Winkler, M. Hellwig, G. Ruff, R. Grimm, and J. H. Denschlag, Tuning the Scattering Length with an Optically Induced Feshbach Resonance, *Phys. Rev. Lett.* **93**, 123001 (2004).
- [39] S. K. Adhikari, Bright dipolar Bose-Einstein-condensate soliton mobile in a direction perpendicular to polarization, *Phys. Rev. A* **90**, 055601 (2014).
- [40] R. Nath, P. Pedri, and L. Santos, Phonon Instability with Respect to Soliton Formation in Two-Dimensional Dipolar Bose-Einstein Condensates, *Phys. Rev. Lett.* **102**, 050401 (2009).
- [41] C. Ticknor, R. M. Wilson, and J. L. Bohn, Anisotropic Superfluidity in a Dipolar Bose Gas, *Phys. Rev. Lett.* **106**, 065301 (2011).
- [42] S. K. Adhikari, Demixing and symmetry breaking in binary dipolar Bose-Einstein-condensate solitons, *Phys. Rev. A* **89**, 013630 (2014).
- [43] V. E. Zakharov and L. A. Ostrovsky, Modulation instability: The beginning, *Physica D* **238**, 540 (2009).

- [44] G. Biondini and D. Mantzavinos, Universal Nature of the Non-linear Stage of Modulational Instability, *Phys. Rev. Lett.* **116**, 043902 (2016).
- [45] W. Królikowski, O. Bang, and J. Wyller, Modulational instability in nonlocal nonlinear Kerr media, *Phys. Rev. E* **64**, 016612 (2001).
- [46] W. Królikowski, O. Bang, N. I. Nikolov, D. Neshev, J. Wyller, J. J. Rasmussen, and D. Edmundson, Modulational instability, solitons and beam propagation in spatially nonlocal nonlinear media, *J. Opt. B* **6**, S288 (2004).
- [47] For repulsive interactions between atoms, the MI can result in the emergence of supersolid behaviors in dipolar BECs [24–27]. The result given by Fig. 2(g) indicates that the domain for the occurrence of supersolids in the dipolar BEC will be reduced by the introduction of the quantum fluctuations.
- [48] Y. V. Kartashov, V. M. Lashkin, M. Modugno, and L. Torner, Spinor-induced instability of kinks, holes and quantum droplets, *New J. Phys.* **24**, 073012 (2022).
- [49] D. S. Petrov and G. E. Astrakharchik, Ultradilute Low-Dimensional Liquids, *Phys. Rev. Lett.* **117**, 100401 (2016).